PAPER • **OPEN ACCESS**

New horizons in quantitative compositional mapping – Analytical conditions and data reduction using XMapTools

To cite this article: P Lanari and F Piccoli 2020 *IOP Conf. Ser.: Mater. Sci. Eng.* **891** 012016

IOP Conf. Series: Materials Science and Engineering **891** (2020) 012016 doi:10.1088/1757-899X/891/1/012016

New horizons in quantitative compositional mapping – Analytical conditions and data reduction using XMAPTOOLS

P Lanari and F Piccoli

University of Bern, Institute of Geological Sciences, Baltzerstrasse 1+3, 3012 Bern, Switzerland

E-mail: pierre.lanari@geo.unibe.ch

Abstract. Quantitative compositional mapping is a key technique for imaging solids and, therefore, for trying to understand compositional zoning systematics in a broad range of geological materials. Compositional mapping requires an adapted analytical method for efficient data collection, a post-processing calibration stage to obtain elemental concentration values, and specific computer tools for exploring and visualising the data. In this contribution, we describe optimal analytical conditions, possible physical limitations and data reduction strategies for compositional maps of major, minor and trace elements obtained by electron probe microanalysis (EPMA) and laser ablation inductively-coupled plasma mass spectrometry (LA-ICP-MS). Data reduction is performed using the computer software XMAPTOOLS, which incorporates a large variety of options and tools for data processing, data calibration and data visualisation based on single and multi-channel maps or via binary, ternary and spider diagrams.

1. Introduction

Rock samples typically exhibit complex textures, mineral distributions and/or compositional zoning requiring chemical analysis of major, minor and trace elements over mm- to cm-sized areas. This 'natural constraint' fostered the development of analytical techniques [1-4] and software solutions [5-9] for obtaining maps of element concentration in solid geological materials. The two most popular scientific techniques for compositional mapping are electron probe microanalysis (EPMA) for major to minor elements and laser ablation inductively-coupled plasma mass spectrometry (LA-ICP-MS) for trace elements. In practice, these two mapping techniques have both advantages and disadvantages – they are complementary rather than substitutes for one another [10]. As we shall demonstrate in the following, the major advantage of EPMA lies in its high spatial resolution, in the range of 1 - 10 μm^3, whereas LA-ICP-MS analyses involve much larger analytical volumes (> 100 μm^3) but with the power of detecting small compositional variations of critical trace elements at the ppm level. However, both techniques require specific data reduction schemes for data correction, calibration and visualisation. In this study, we present recent improvements of XMAPTOOLS [6, 11] (available via https://www.xmaptools.com), an advanced software toolbox especially designed to achieve optimum workflow and feature extraction from compositional maps of rock samples. This software solution can readily handle maps obtained from a large variety of instruments including both EPMA and LA-ICP-MS (e.g., [6, 12]).

Quantitative compositional mapping by EPMA has become a routine technique in many laboratories worldwide. It requires the acquisition of X-ray maps (i.e., raw data not corrected for background or matrix effects) measured at specific X-ray emission lines and a post-collection calibration stage called analytical standardisation to derive fully quantitative data of element concentrations. The calibration can be performed either based on an empirical or semi-empirical correction schemes [1-3] or against internal standards assuming no matrix effects [4]. The advantages and limits of each strategy are discussed in Lanari *et al.* [6]. The internal standardisation procedure implemented in XMAPTOOLS [11] requires high-precision spot analyses of every mineral phase to be calibrated. This technique was improved by adding a pseudo-background correction [6].

Quantitative compositional mapping of trace elements and isotopes by LA-ICP-MS is catching up. It started with the seminal study of Woodhead *et al.* [13] and has improved at a fast rate in the past 10 years. Mapping by LA-ICP-MS involves the acquisition of successive raster images of the focussed laser beam. Each acquisition line is calibrated using a standard reference glass and a known element concentration as internal standard. The calibrated data are then stitched together to form compositional maps of trace element distributions. The calibration is usually performed using the modules available within the commercial software IOLITE [14-16], whereas subsequent image processing and data visualisation is easier and more flexible if done with XMAPTOOLS [12].

2. Analytical conditions

This section briefly outlines some important aspects of each analytical procedure along with recommended instrument operating conditions. Common artefacts affecting the spatial and chemical resolutions that were not investigated in previous studies (e.g., [4, 6, 11, 12]) are further discussed.

2.1. Quantitative compositional mapping by EPMA

A standard analytical setup for quantitative compositional mapping of silicates and oxides by EPMA is presented in Table 1. This setup is optimised for modern EPMA instruments equipped with five wavelength-dispersive X-ray spectrometers (WDS) and a single energy-dispersive X-ray spectrometer (EDS). The final image resolution is defined according to the total number of pixels of a map: low resolution for an image containing less than 150,000 pixels; medium resolution between 150,000 and 500,000 pixels; and high resolution above 500,000 pixels. The area of interest on the specimen is scanned via mechanical beam tracking mode, i.e., by moving the sample under a static electron beam using a high-precision computer-controlled x-y-z stage. In practice, the accelerating voltage of the electron beam is fixed at 15 keV, as it is for 'typical' spot analyses. The specimen current, measured at the Faraday cup, is increased up to at least 100 nA to compensate the short dwell times (Table 1). The characteristic X-ray emission caused by beam-specimen interaction is continuously analysed using both WDS and EDS spectrometers, resulting in the acquisition of 15 to 20 elemental maps in two acquisitions (as only five elements can be measured by WDS, the area is often scanned twice). The measurement time for a single area of interest takes between one night and few days, depending on the image resolution and the dwell time.

Two effects are further discussed in the following: (1) the size of the interaction volume, which can result in overlapping effects or under-sampling of a specific mineral and (2) beam damage during analysis. Other potential artefacts such as secondary fluorescence effects, thermal or beam current instability, spectrometer focus and surface irregularities are discussed in Lanari *et al.* [6].

2.1.1. Interaction volume and spatial resolution. In compositional mapping by EPMA, the spatial resolution is determined by the spacing of spot measurements and the X-ray excitation volume of the electron beam. The pixel size *dx* in the final image is equal to the distance between two spots. Any interaction volume larger than *dx* results in overlapping, increasing the number of mixed pixels, which

Table 1. Standard analytical setup for quantitative compositional mapping by EPMA.

	Setup 1 (medium resolution)	**Setup 2 (high resolution)**
Accelerating voltage (keV)	15	
Beam current (nA)	100 (eventually up to 500)	
Map size in pixels (# pixels)	500 × 500 (250,000)	1,000 × 1,000 (1,000,000)
Step size (µm)	1 - 40	
Map surface (mm^2)	0.25 - 400	1 - 1,600
Dwell time (ms)	100 - 300	60 - 200
Map acquisitions	2	
# elements WDS	10 (e.g., Si-Kα, Ti-Kα, Al-Kα, Fe-Kα, Mn-Kα, Mg-Kα, Ca-Kα, Na-Kα, K-Kα, Cr-Kα/Ni-Kα)	
# elements EDS	5 - 10 (e.g., P-Kα, S-Kα, Zr-Kα, Ce-Lα, La-Lα, etc.)	
Mapping time (h)	14 - 42	33 - 112

are pixels having a mixed composition between two or more phases. In contrast, any interaction volume smaller than *dx* results in under sampling and may cause small phases to be missed. It is, therefore, critical to quantitatively evaluate the size of the excitation volume for a large variety of minerals.

Electron-specimen interaction volumes were investigated using a Monte Carlo model and the computer programme CASINO 2.41 [17] for a set of 14 common rock-forming minerals including garnet (almandine ρ = 4.19 $g.cm^{-3}$; Z = 15.6), clinopyroxene (omphacite ρ = 3.34 $g.cm^{-3}$; Z = 14.6), white mica (muscovite ρ = 2.82 $g.cm^{-3}$; Z = 11.32), feldspar (albite ρ = 2.62 $g.cm^{-3}$; Z = 11.73), amphibole (glaucophane ρ = 3.34 $g.cm^{-3}$; Z = 10.6), calcite (ρ = 2.71 $g.cm^{-3}$; Z = 12.6), olivine (forsterite ρ = 3.27 $g.cm^{-3}$; Z = 10.6; fayalite ρ = 4.39 g.cm-3; Z = 18.7), epidote (zoizite ρ = 3.30 g.cm-3; Z = 12.1), chlorite (clinochlore ρ = 2.65 $g.cm^{-3}$; Z = 12.2), kyanite (ρ = 3.61 $g.cm^{-3}$; Z = 10.7), magnetite (ρ = 5.15 $g.cm^{-3}$; Z = 21.0), quartz (ρ = 2.62 $g.cm^{-3}$; Z = 10.8), and orthopyroxene (ferrosilite ρ = 3.95 $g.cm^{-3}$; Z = 14.2). The accelerating voltage and beam diameter were kept constant at 15 keV and 1 µm. A selection of four representative cases is presented in Fig. 1. The maximum diameter of the interaction volume *d* was estimated for each mineral from the trajectories of 10,000 simulations using a home-made routine defining a 95 % confidence interval of successive layers (cylinder shape) with a thickness of 0.2 µm between 0 and 2 µm depth and 0.5 µm below 2 µm depth. This maximum diameter of the interaction volume decreases with increasing mean atomic number *Z* and density *ρ* (unit $g.cm^{-3}$) of the target material (Fig. 2). This trend can be reproduced using the following relation:

$$d = 4.034 \exp(-0.02139\, Z\rho^2) + 1.548 \exp(-0.006457\, Z\rho^2) \quad (1)$$

This equation can be used for approximating a first order maximum diameter of interaction volume in common silicates and oxides at 15 keV and 1 µm beam diameter and may, therefore, assist in the interpretation of compositional maps. This technique was implemented in XMAPTOOLS 3.0.1; two application examples based on published datasets are presented in Fig. 3.

The purpose of the first dataset was to derive local bulk compositions to be used in thermodynamic models [18]. An area of 12.3 mm × 12.3 mm was analysed with a step size of 12 µm resulting in an image size of 1024 × 1024 pixels corresponding to 1,048,567 fully quantitative analyses. Only a small portion of this map was re-investigated here (Fig. 3a). The major drawback of this setup is that the electron-specimen interaction volume is much smaller than the pixel size (Figs. 3a to 3c). The resulting under sampling effect is strong as the analysed pseudo-surface ranges between 1 % (garnet) and 5 % (plagioclase) of the pixel surface in the final image (Fig. 3c). In this example, the average grain

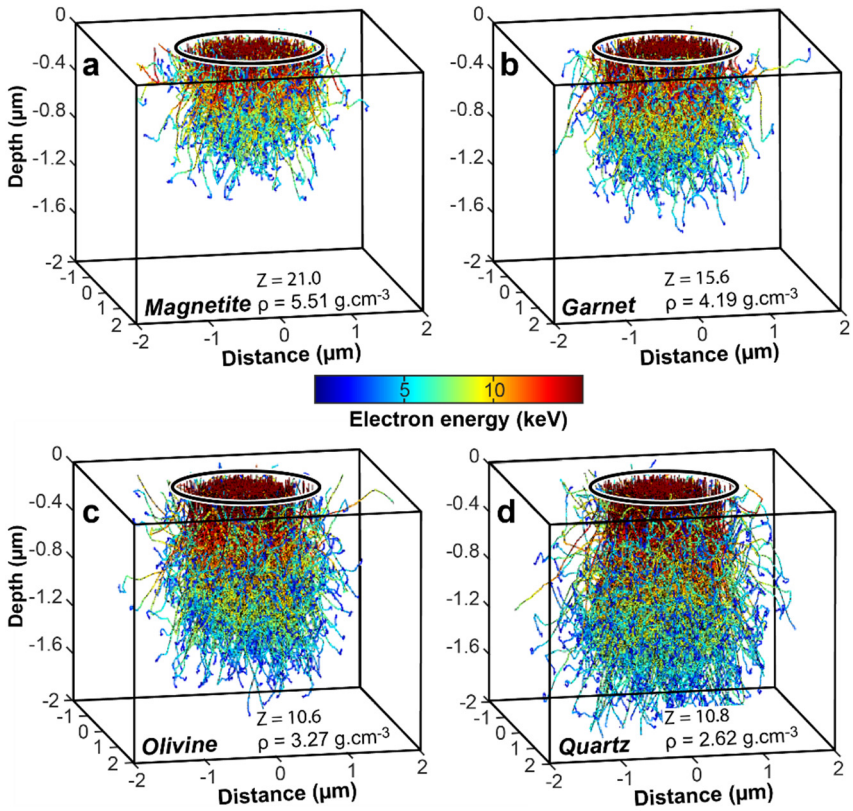

Figure 1. Illustration of possible electron-specimen interaction in four rock-forming minerals covering a broad spectrum of mean atomic number ($_Z$) and density ($_\rho$). A total of 10,000 simulations were performed for each mineral using the programme CASINO 2.41 (see text), but only a selection of 1,000 trajectories is shown in this figure. The size of the excitation volume is increasing with decreasing values of Z and ρ as also shown by Eq. (1). Colours show the energy of the electron (in keV). The black circle shows the beam size at the sample surface.

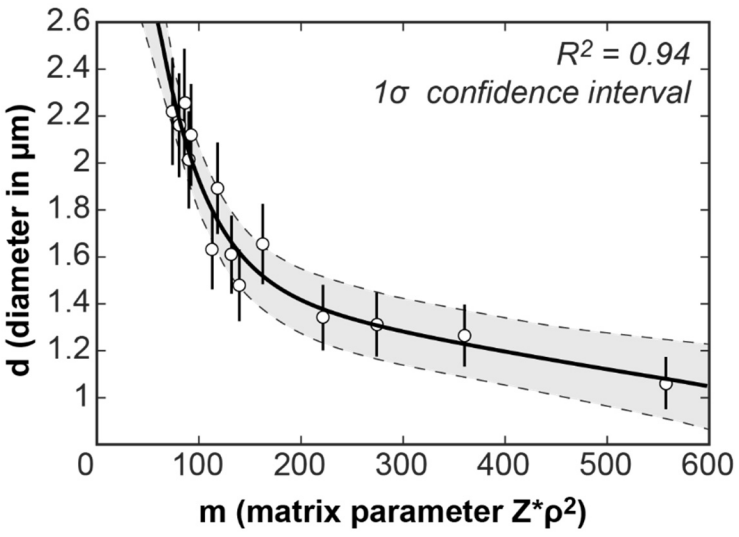

Figure 2. Diameter of electron-specimen interaction volume as a function of a matrix parameter m defined as the product of the mean atomic number (Z) and the square of the density (ρ^2) of the material. A bi-exponential model corresponding to the sum of two exponential functions was used for fitting (see Eq. (1)). The uncertainty on the value of d obtained by the Monte Carlo technique was arbitrary fixed to 10 %. Note that these data points were generated for an accelerating voltage of 15 keV and a spot size of 1 µm.

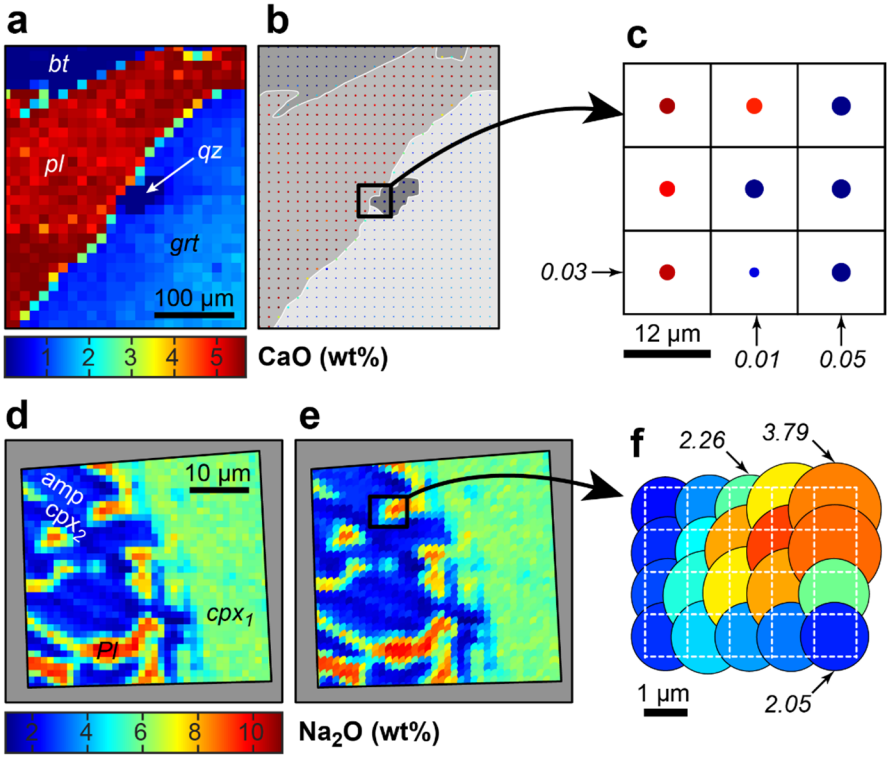

Figure 3. Possible effects of the pixel size (*dx*) on the spatial resolution of X-ray maps with a beam size of 1 µm. a) Small area of a CaO map (in wt%) with a step size of 12 µm obtained for a high-grade metamorphic rock from the Central Himalaya (modified from [18]). b) Image with circle pixels representing the electron-specimen interaction volume (see Eq. 1). Garnet has a smaller interaction volume than quartz (Fig. 1). c) Detailed view illustrating the under sampling effect. The numbers correspond to the diameter of the interaction volume (in µm) calculated for a specific pixel. d) Small area of a Na_2O map (in wt%) with a step size of 1 µm obtained for an eclogite from the NW Himalaya (modified from [21]). e) Image with circle pixels representing the electron-specimen interaction volume. f) Detailed view illustrating the overlapping effect. The numbers correspond to the diameter of the interaction volume (in µm) calculated for a specific pixel. Abbreviations: bt - biotite; pl - plagioclase; qz - quartz; grt - garnet; cpx clinopyroxene; amp - amphibole.

size is much larger than the step size and under sampling does not affect significantly the local bulk composition estimates. However, small phases (5 - 10 µm width) might not be analysed with this setup. Increasing the beam diameter to the same value of the step size improves the detection of small phases (e.g., [19, 20]), but significantly increases the number of mixed pixels and is, therefore, less suitable for quantitative analysis of zoned materials.

The second dataset shows an opposite case in which the electron-specimen interaction volume is larger than the pixel size (Figs. 3d to 3f). An area of 0.52 mm × 0.67 mm was analysed with a step size of 1 µm corresponding to 348,400 fully quantitative analyses [21]. Over sampling increases significantly the number of mixed pixels. In Fig. 3c, only one pixel shows the true composition of Na_2O in plagioclase, whereas a two-pixel rim exhibits mixed compositions towards amphibole or clinopyroxene. The degree of over sampling ranges between 200 % for clinopyroxene (cpx2) and 400 % for plagioclase. Mixed pixels are the main source of misclassification and are challenging to calibrate. These two examples show that a good compromise for the analysis of geological materials is a step size of ~2 µm.

2.1.2. Beam damage. The electron beam exposure produces heat over time and this heat can drive element diffusion in the target material. In addition, the trapping of electrons can generate an electric field within the sample and cause migration of positive ions toward a region of negative charge located outside of the analysis volume. These effects known as beam damage can significantly affect the content and distribution of mobile elements during the acquisition of spot analyses and mapping. Beam-induced changes in composition generally cause the X-ray intensity of mobile elements such as Na, Ca and K to decrease (diffusion out) and heavier element to slightly increase due to changes in density and the absorption behaviour of the specimen.

A meta-quartzite from the Glacier-Rafray Klippe in the Western Alps [22] was used to illustrate the possible effects of sample alteration during mapping under an electron beam with high-current conditions. A small area of 80 × 120 μm^2 containing albite, muscovite and quartz was mapped five times (two acquisitions each corresponding to a total of 10 scans) at the Institute of Geological Sciences of the University of Bern using a JEOL-820 Superprobe instrument, an accelerating voltage of 15 keV, a beam current of 200 nA, a beam size of 1 μm and 200 ms dwell time. The series of X-ray maps for Na-, K- and Al-Kα lines uncorrected for background are shown in Fig. 4. The mobile elements are affected by beam damage. In albite, between 5 and 35 % of the total Na-Kα counts were lost after two scans (Fig. 4b), this figure rises up to > 90 % after 9 scans (Fig. 4e). Although the original distribution of Na in albite was homogenous, this is not the case after beam damage demonstrating that diffusion was not homogenous throughout. A moderate amount of Na is preserved in bright spots 5 μm thick (Figs. 4c to 4e). In muscovite, K is more resilient to diffusion under the high-current electron beam and the K-Kα signal experienced only < 10 % count loss after two scans (Fig. 4g) and 50 - 60 % after 9 scans (Fig. 4j). In this case, the compositional zoning of muscovite is preserved (Figs. 4f and 4e). It is important to notice that in plagioclase, Al-Kα count rate increases up to 10 % in the areas with high Na diffusion (e.g., between Fig. 4k and Fig. 4o).

This example shows that beam damage can significantly affect the count rates obtained during mapping. Therefore, mobile elements (Na, K, Ca) have to be measured during the first pass of the beam over the mapped area and after the acquisition of spot analyses for calibration. It is also important to notice that beam damage caused by spot analyses can result in a significant overestimation in the concentration of the element after calibration.

2.2. Quantitative compositional mapping by LA-ICP-MS

A standard analytical setup for quantitative compositional mapping of silicates such as garnet by LA-ICP-MS is presented in Table 2. This setup is optimized for a 193 nm exciter laser coupled to a quadrupole ICP-MS. Mapping can be performed on standard polished thin sections or epoxy mounts. The area of interest is scanned using parallel rasters analysed across the sample surface. A single raster analysis is preceded by 20 - 30 s background analysis and a pre-ablation stage with larger laser beam size followed by 10 s pre-washout. The pre-ablation aims to minimise re-deposition effects. Standards (including standard reference materials such as glasses SRM610 and SRM612) are analysed at the start and end of each mapping run and every 0.5 to 1 h during mapping. The measurement time for a single area of interest takes between few hours and few days, depending on the size of the area (Table 2).

3. Data reduction using XMAPTOOLS

This section briefly summarises the main workflow procedures implemented in XMAPTOOLS (see also [6, 11]).

3.1. Workflow for EPMA data

Step 1 – Importing raw data and corrections. Corrections applied to X-ray maps include a dead time correction for deriving true count rates, correction for intensity deviations caused by sample surface topography and/or time-dependent drift. The corrections applied to the spot analyses (which are used as internal standard) include the elimination of mixed compositions and the adjustment of position (caused by sample displacement during the analysis) based on statistical criteria.

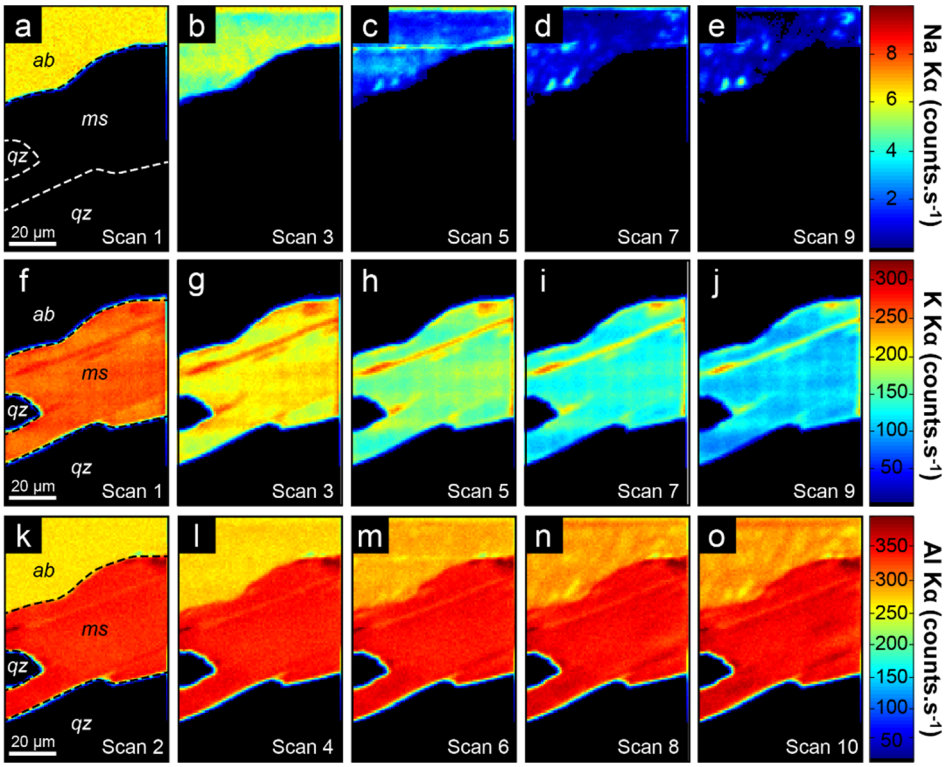

Figure 4. Beam damage effects in albite and muscovite from a meta-quartzite (Glacier-Rafray Klippe, Western Alps). The count rates (unit counts per second) of mobile elements Na and K in albite and muscovite progressively decrease with time (from left to right) because of beam damage. Note that the count rates of Al in both plagioclase and muscovite are increasing from left to right. Mineral abbreviations: ab - albite; ms - muscovite; qz - quartz.

Table 2. Standard analytical setup for quantitative compositional mapping of garnet by LA-ICP-MS.

	Setup 1 (small resolution)	**Setup 2 (medium resolution)**
Laser wavelength (nm)	193	
Fluence (energy density, J.cm^{-2})	5 - 7	
Repetition rate (Hz)	10	
Sampling mode	rastering	
Carrier and make-up gases (L.min^{-1})	He (0.5 - 0.7) and Ar (0.9 L.min^{-1})	
Map size in pixels (# pixels)	100 × 100 (10,000)	300 × 300 (90,000)
Laser spot diameter (µm)	16 - 24	
Map surface (mm^2)	1.6 × 1.6	4.8 × 4.8
Scan speed (µm.s^{-1})	22 - 30	
Dwell time (ms) (elements)	10 - 20 ms (Sr, Y, Zr, La, Ce, Pr, Nd, Sm, Eu, Gd, Tb, Dy … Ho, Er, Tm, Lu, Th, U) 5 - 10 ms (Na, Mg, Si, P, K, Ca, Ti, Cr, Mn, Fe)	
Total sweep time (s)	0.30 - 0.5	
Mapping time (h)	5 - 7	24 - 36

Step 2 – Multi-channel classification (and manual phase identification). An automated technique based upon the K-means algorithm is implemented in XMAPTOOLS. Alternatively, a step-by-step manual classification can be performed using the modules *BINARY* or *TRIPLOT*. Individual masks are created from a range of composition defined graphically [11]. An example of manual classification is shown in Fig. 5. Four masks were generated from the binary Mg versus Al. This manual procedure allows the mixed pixels to be excluded (see grey points in Fig. 5a and the corresponding black pixels in Fig. 5c). Excluding mixed pixels is important for obtaining high quality chemical images, such as maps of structural formulas. An automated algorithm eliminating the pixels located between the different masks is also provided in XMAPTOOLS (BRC correction, see [6]).

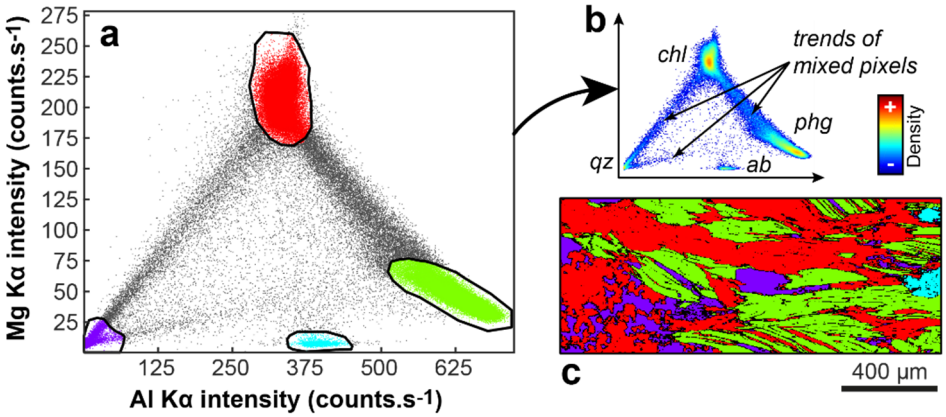

Figure 5. Manual classification in XMAPTOOLS via the BINARY module using a compositional map of a low-temperature high-pressure metasediment from the Western Alps (Briançonnais). a) Binary diagram Mg versus Al (unit: counts per second); each point corresponds to the composition of a single pixel. Selection of four groups using the option 'multi-group free shape'. The grey pixels are mixed pixels and are not classified in this example. b) Density map of the binary diagram shown in (a). c) Map showing the spatial distribution of the pixels of each group selected in (a). Abbreviations: chl - chlorite; qz - quartz; phg - phengite; ab albite.

Step 3 – Analytical standardisation. The module *STANDARDIZATION* assists the user for the calibration of the elements of each phase. An automated routine uses the variability of the mass concentration of the spot analyses to fit the slope of the calibration curve and approximate the background intensity (see Fig. 7 in [6]). The position of the calibration curve can also be manipulated manually.
Step 4 – Data exploration and visualisation. Once the maps have been calibrated, the data can be plotted as single or multi-channel maps or in binary, ternary and spider diagrams. XMAPTOOLS provides a guided environment for data exploration based on a large variety of structural formulas, diagnostic elemental ratios for major and trace elements as well as temperature and pressure conditions.

3.2 Workflow for LA-ICP-MS data
Step 1 – Importing data and corrections. The LA-ICP-MS data are imported in XMAPTOOLS as element concentration either in ppm or weight percentage of element [12]. The map size and orientation can be adjusted in the module *IMPORT TOOLS*. Holes, polish defects and all other mineral phases are masked-out using one of the classification options described above.
Step 2 – Trace element map visualisation and sampling tools. (Note that these tools are available for the analysis of any type of map, including EPMA data). XMAPTOOLS incorporates several options for

data visualisation specially designed for trace element analysis. The element concentration can be displayed using either linear or logarithmic colour bar (Figs. 6a and 6b). The compositions can be extracted along any linear profile or path and plotted for all or a selection of elements (Fig. 6c). Average compositions and associated standard deviations can be extracted from spatial domains (area-of-interest) or along a smoothed profile – integrating a rectangular area or using a scanning window.

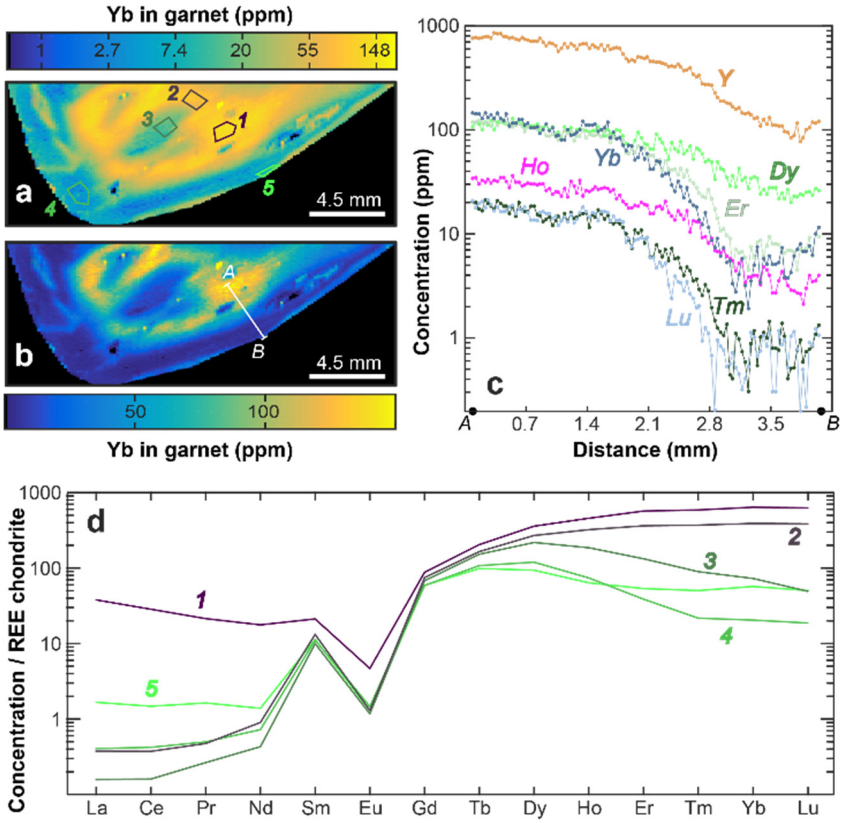

Figure 6. Garnet LA-ICP-MS map from a migmatite of the El Oro Metamorphic Complex (SW Ecuador) showing complex trace element distribution patterns. Map of Yb (in ppm) plotted using a) logarithmic, and b) linear colour scales. c) Trace element concentration profile from A to B; note that the position of the profile is shown in (b). c) Chondrite-normalised rare earth element (REE) patterns for five areas reported in (a). This diagram depicts the behaviour of REE in each zone.

Step 3 – Trace element data visualisation, spider diagrams and map transformation. Similarly to major element, trace element data can be visualised using the modules *BINARY* and *TRIPLOT*. Manual and automated clustering allow chemical groups and their spatial distribution to be characterised. Spider diagrams – plots of the abundances of a set of elements such as rare earth elements (REE) relative to their abundance in some standard – can be readily generated in XMAPTOOLS using the one of the sets of normalisation values available (Fig. 6d). Finally, the maps can be combined together within the *GENERATOR* module using any arithmetic operation generating a new map.

Acknowledgements
We thank an anonymous reviewer for providing suggestions that improved the clarity of the paper as well as Bjørn E. Sørensen and Luc Van 't dack for their efficient editorial handling.

References

[1] Cossio R and Borghi A 1998 PETROMAP: MS-DOS software package for quantitative processing of X-ray maps of zoned minerals. *Comp. Geosci.* **24** 805-814
[2] Clarke G L, Daczko N R and Nockolds C 2001 A method for applying matrix corrections to X-ray intensity maps using the Bence-Albee algorithm and Matlab. *J. Metamorphic Geol.* **19** 635-644
[3] Chouinard J and Donovan J 2015 Quantitative elemental mapping with electron microprobe and automated data analysis. *Microsc. Microanal.* **21** 2193-2194
[4] De Andrade V, Vidal O, Lewin E, O'Brien P and Agard P 2006 Quantification of electron microprobe compositional maps of rock thin sections: an optimized method and examples. *J. Metamorphic Geol.* **24** 655-668
[5] Lanari P, Wagner T and Vidal O 2014 A thermodynamic model for di-trioctahedral chlorite from experimental and natural data in the system MgO–FeO–Al2O3–SiO2–H2O: applications to P-T sections and geothermometry. *Contr. Mineral. Petrol.* **167** 968
[6] Lanari P, Vho A, Bovay T, Airaghi L and Centrella S 2019 Quantitative compositional mapping of mineral phases by electron probe micro-analyser. in: *Metamorphic geology: Microscale to mountain belts*. (Ferrero S, Lanari P, Goncalves P and Grosch E G; Eds.). *Geol. Soc. London Spec. Publ.* **478**, 39-63
[7] Ortolano G, Zappalà L and Mazzoleni P 2014 X-ray map analyser: A new ArcGIS® based tool for the quantitative statistical data handling of X-ray maps (Geo- and material-science applications). *Comp. Geosci.* **72** 49-64
[8] Ortolano G, Visalli R, Godard G and Cirrincione R 2018 Quantitative X-ray map analyser (Q-XRMA): A new GIS-based statistical approach to mineral image analysis. *Comp. Geosci.* **115** 56-65
[9] Tinkham D K and Ghent E D 2005 XRMapAnal: A program for analysis of quantitative X-ray maps. *Amer. Mineralogist* **90** 737-744
[10] Lanari P and Engi M 2017 Local bulk composition effects on mineral assemblages. *Rev. Mineral. Geochem.* **83** 55-102
[11] Lanari P, Vidal O, De Andrade V, Dubacq B, Lewin E, Grosch E G and Schwartz S 2014 XMapTools: A MATLAB©-based program for electron microprobe X-ray image processing and geothermobarometry. *Comp. Geosci.* **62** 227-240
[12] Raimondo T, Payne J, Wade B, Lanari P, Clark C and Hand M 2017 Trace element mapping by LA-ICP-MS: assessing geochemical mobility in garnet. *Contr. Mineral. Petrol.* **172** 17
[13] Woodhead J D, Hellstrom J, Hergt J M, Greig A and Maas R 2007 Isotopic and elemental imaging of geological materials by laser ablation inductively coupled plasma-mass spectrometry. *Geostand. Geoanal. Res.* **31** 331-343
[14] Paul B, Paton C, Norris A, Woodhead J, Hellstrom J, Hergt J and Greig A 2012 CellSpace: A module for creating spatially registered laser ablation images within the Iolite freeware environment. *J. Anal. Atom. Spectrom.* **27** 700-706
[15] Paul B, Woodhead J D, Paton C, Hergt J M, Hellstrom J and Norris C A 2014 Towards a method for quantitative LA-ICP-MS imaging of multi-phase assemblages: Mineral identification and analysis correction procedures. *Geostand. Geoanal. Res.* **38** 253-263
[16] Petrus J A, Chew D M, Leybourne M I and Kamber B S 2017 A new approach to laser-ablation inductively-coupled-plasma mass-spectrometry (LA-ICP-MS) using the flexible map interrogation tool 'Monocle'. *Chem. Geol.* **463** 76-93
[17] Drouin D, Couture A R, Joly D, Tastet X, Aimez V and Gauvin R 2007 CASINO V2.42 - Fast and easy-to-use modeling tool for scanning electron microscopy and microanalysis users. *Scanning* **29** 92-101
[18] Lanari P and Duesterhoeft E 2019 Modeling metamorphic rocks using equilibrium thermodynamics and internally consistent databases: Past achievements, problems and perspectives. *J. Petrology* **60** 19-56

[19] Williams M L, Jercinovic M J, Mahan K H and Dumond G 2017 Electron microprobe petrochronology. *Rev. Mineral. Geochem.* **83** 153-182
[20] Yasumoto A, Yoshida K, Kuwatani T, Nakamura D, Svojtka M and Hirajima T 2018 A rapid and precise quantitative electron probe chemical mapping technique and its application to an ultrahigh-pressure eclogite from the Moldanubian Zone of the Bohemian Massif (Nové Dvory, Czech Republic). *Amer. Mineralogist* **103** 1690-1698
[21] Lanari P, Riel N, Guillot S, Vidal O, Schwartz S, Pêcher A and Hattori K H 2013 Deciphering high-pressure metamorphism in collisional context using microprobe mapping methods: Application to the Stak eclogitic massif (northwest Himalaya). *Geology* **41** 111-114
[22] Burn M 2016 *LA-ICP-QMS Th-U/Pb allanite dating: methods and applications*. PhD-thesis. (Bern, Switzerland: University of Bern) 399